Biomicrofluidics ARTICLE pubs.aip.org/aip/bmf

Photonic crystal enhanced immunofluorescence biosensor integrated with a lateral flow microchip: Toward rapid tear-based diabetic retinopathy screening

Cite as: Biomicrofluidics **17**, 044102 (2023); doi: 10.1063/5.0158780
Submitted: 17 May 2023 · Accepted: 10 July 2023 ·
Published Online: 20 July 2023

Li-Ying Chen,[1] Sheng-Min Hsu,[2] Jhih-Cheng Wang,[3,4,a)] Tai-Hua Yang,[1,5] and Han-Sheng Chuang[1,6,a)]

AFFILIATIONS

[1]Department of Biomedical Engineering, National Cheng Kung University, Tainan, Taiwan
[2]Department of Ophthalmology, National Cheng Kung University Hospital, Tainan 701, Taiwan
[3]Department of Urology, Chimei Medical Center, Tainan, Taiwan
[4]Department of Electric Engineering, Southern Taiwan University of Science and Technology, Tainan, Taiwan
[5]Department of Orthopedic Surgery, National Cheng Kung University Hospital, Tainan, Taiwan
[6]Medical Device Innovation Center, National Cheng Kung University, Tainan, Taiwan

[a)]**Authors to whom correspondence should be addressed:** tratadowang@gmail.com and oswaldchuang@mail.ncku.edu.tw

ABSTRACT

Diabetic retinopathy (DR) has accounted for major loss of vision in chronic diabetes. Although clinical statistics have shown that early screening can procrastinate or improve the deterioration of the disease, the screening rate remains low worldwide because of the great inconvenience of conventional ophthalmoscopic examination. Instead, tear fluid that contains rich proteins caused by direct contact with eyeballs is an ideal substitute to monitor vision health. Herein, an immunofluorescence biosensor enhanced by a photonic crystal (PhC) is presented to handle the trace proteins suspended in the tear fluid. The PhC was constructed by self-assembled nanoparticles with a thin layer of gold coated on top of it. Then, the PC substrate was conjugated with antibodies and placed in a microchannel. When the capillary-driven tear sample flew over the PC substrate, the immunoassay enabled the formation of a sandwich antibody-antigen-antibody configuration for PhC-enhanced immunofluorescence. The use of PhC resulted in a concentration enhancement of more than tenfold compared to non-PhC, while achieving an equivalent signal intensity. The limit of detection for the target biomarker, lipocalin-1 (LCN-1), reached nearly 3 μg/ml, and the turnaround time of each detection was 15 min. Finally, a preclinical evaluation was conducted using ten tear samples. A clear trend was observed, showing that the concentrations of LCN-1 were at least twofold higher in individuals with chronic diabetes or DR than in healthy individuals. This trend was consistent with their medical conditions. The results provided a direct proof-of-concept for the proposed PhC biosensor in rapid tear-based DR screening.

I. INTRODUCTION

The low screening rate (<30%) of diabetic retinopathy (DR)[1,2] has raised concern for major loss of vision in the diabetic population worldwide annually. To date, the mostly practiced DR screening procedure in clinics often requires patients to undergo mydriasis to dilate their pupils and then be examined under ophthalmoscopy by a clinical specialist, which is very time-consuming, tedious, and labor-intensive. Moreover, the diagnosis is heavily dependent on the examiner's subjective judgment, thereby resulting in possible human errors and sometimes unreliability. Alternatively, fluorescein angiography (FAG) and optical coherent tomography (OCT) are two advanced methods that improve long waiting and reliability. Nevertheless, FAG remains an invasive examination that requires injecting a fluorescein agent into the patient's retinal bloodstream while OCT is too costly to afford in every clinic despite providing more detailed retinal information. In

addition, the examiner's experience plays a key factor in the diagnosis considering that both FAG and OCT lack quantitative information. Lately, the integration of a miniaturized objective lens and a smartphone has shed light on point-of-care testing.[3] This portable device allows patients to perform examination at home and consult with their ophthalmologist online without the need for clinical visits. Some research[4] even incorporated artificial intelligence to assist identification, thereby enabling a preliminary suggestion to be made onsite. However, all these devices still face challenges of instability because of their hand-held nature.[5,6] Hence, recent precise diagnostics have been developed based on biomarker proteins in tear fluids to avoid the abovementioned problem. In 2019, Sempionatto *et al.*[7] reported an eyeglasses-based tear biosensor for the noninvasive detection of alcohol, vitamins, and glucose. A microfluidic electrochemical detector was integrated into their study with an eyeglasses nose-bridge pad to enable continuous monitoring of some key tear biomarkers. Similarly, another research group[8] achieved simultaneous detection of multiple biomarkers in human tears by a wearable eye-patch biosensor. Herein, different sensing regions on the eye patch were modified with specific chromogenic reagents to selectively determine the *p*H, protein, ascorbic acid, and glucose in the tear. The assay only required 20 μl of tear and a 30-s response time. The limit of detection (LoD) was approximately 0.17 g/l, 7.0 μM, and 3.0 μM for albumin protein, glucose, and ascorbic acid, respectively. A bold project led by Google starting from 2014 also focused on the tear biosensing capability for diabetes but with a contact lens platform.[9] However, the project ceased in 2018 because of a lack of correlation between tear glucose and blood glucose. Nevertheless, the concept of contact lens biosensors remains popular.[10] Similarly, Keum *et al.*[11] grasped the same idea and continued their wireless smart contact lens for diabetes and therapies. Despite the uncertainty, the contact lens seems a good interface worth further explorations for long-term diagnosis of DR. More recently, Wang *et al.*[12] attempted the detection of dual DR biomarker proteins, lipocalin-1 (LCN-1), and VEGF in tears with an optoelectrokinetic microchip. They achieved an optimal LoD down to nearly 100 pg/ml in only 10 s by simply concentrating the trace proteins for the immunofluorescence enhancement. With a pre-calibrated diagram of both biomarkers, they reported 80% accuracy of a clinical test compared with conventional ophthalmoscopic examination. Their follow-up work[13] further advanced the closed configuration to a facile open-well optoelectrokinetic microchip with coplanar electrodes. The new device employed magnetic particles to prevent some washing steps and reached an LoD of as low as 2.9 pg/ml in 1 min. However, the electrochemical and optoelectrokinetic approaches are very limited by medium conditions, surface chemistry, and external facilities. Optoelectrokinetic approaches, such as rapid electrokinetic patterning,[14] require a low-medium conductivity medium (<several tens of mS/m) and a high-frequency driving electric field in combination with a focused light spot. Similarly, electrochemistry is susceptible to electro-migration caused by chemical reactions and the utilization of electrochemical impedance spectroscopy. Therefore, it is crucial to carefully control the chemical reactions to induce redox processes on the electrode surfaces.

In this study, LCN-1, a tear biomarker, was adopted for detection considering the non-invasiveness, high specificity, and high sensitivity in DR.[15–17] The pure optical signal originated from a photonic crystal (PhC) was used to lower the limitations resulting from electrochemistry and optoelectrokinetics (Fig. 1). In addition,

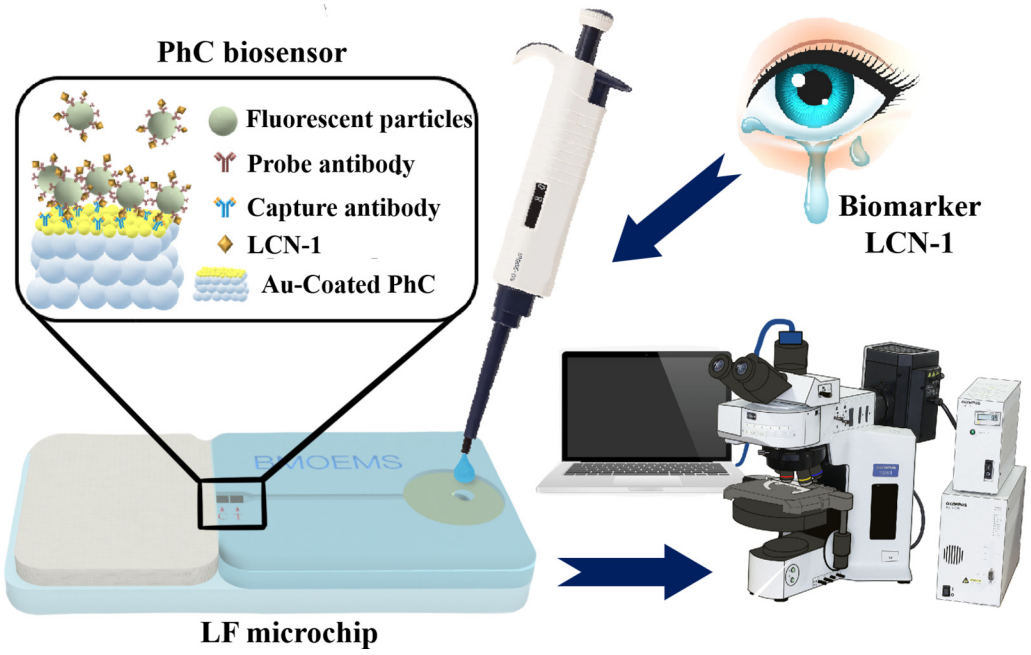

FIG. 1. Conceptual illustration of the tear-based DR screening on an LF microchip-enabled PhC biosensor.

the immunofluorescence was enhanced by the Bragg lattice of PhC. The PhC substrate was made through the self-assembly of 215-nm poly (methyl methacrylate) (PMMA) particles. The substrate was then later embedded in the microchannel of a lateral flow (LF) microchip, wherein tear fluids would be driven by the capillary force. In the presence of the target protein LCN-1, a sandwich immunocomplex labeled with fluorescence would form on the PhC biosensor, thereby resulting in enhanced immunofluorescence and vice versa. The use of PhC resulted in a concentration enhancement of more than tenfold compared to non-PhC, while achieving an equivalent signal intensity. Each detection was completed in 15 min. Furthermore, an optimal LoD of 3 μg/ml for LCN-1 was estimated based on the three-signal criterion. A preclinical evaluation was conducted using ten tear samples from volunteers to demonstrate the proof of concept. The results showed that the concentrations of LCN-1 in cases with chronic diabetes or DR were at least twofold higher than in healthy (i.e., no ocular diseases and diabetes, HbA1c < 6.5%) or non-diabetic (i.e., no diabetes only, HbA1c < 6.5%) cases. This trend was consistent with their medical conditions. The assessments assured the feasibility of the proposed PhC biosensor for future rapid tear-based DR screening and beyond.

II. METHODS AND MATERIALS

A. PMMA nanoparticle self-assembly for a PhC substrate

PhC was used here as a substrate for immunoassays and immunofluorescence enhancement. The self-assembled nanoparticles formed a Bragg's lattice that resonated with the immunofluorescence. The PhC substrate was primarily made up of 215-nm colorless PMMA nanoparticles (PMMA200, Lab261, Palo Alto, CA) [Fig. 2(a)].

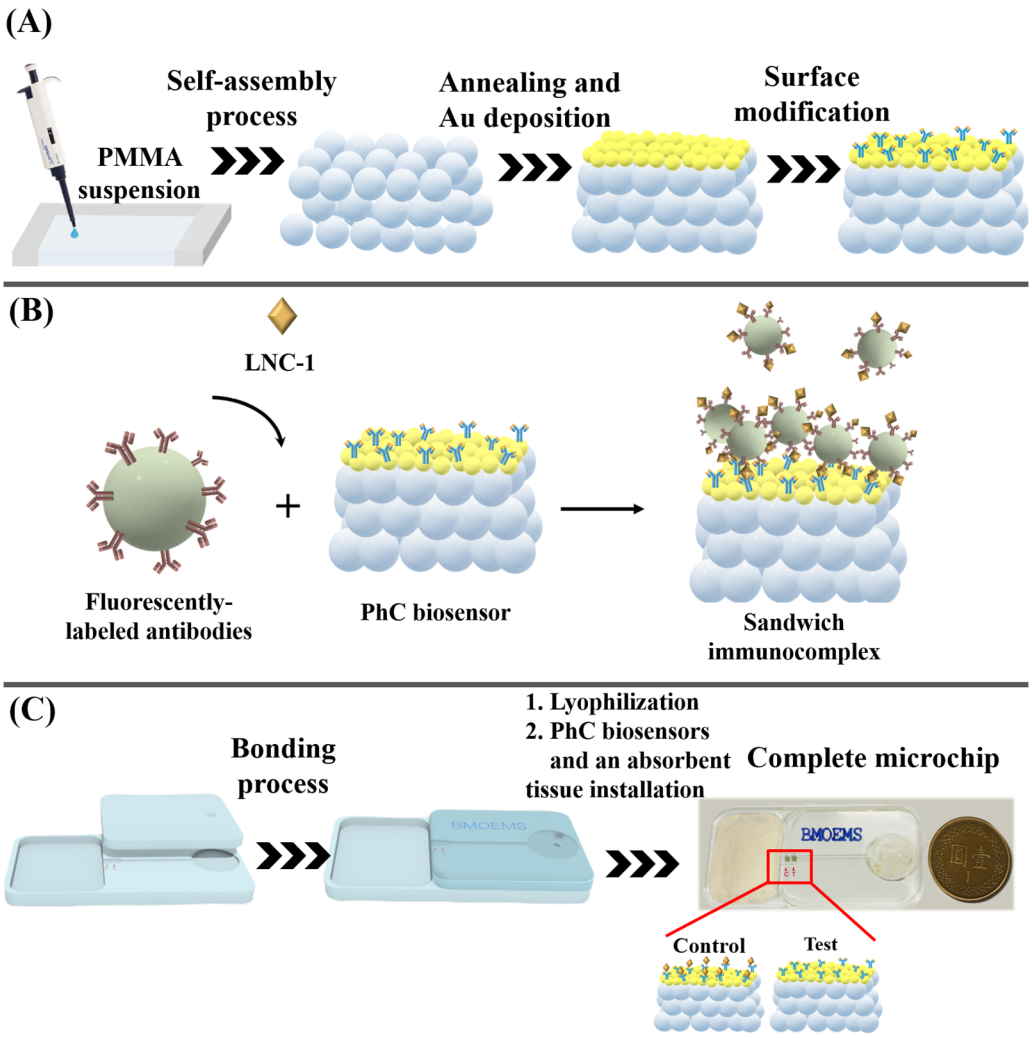

FIG. 2. (a) Fabrication flow chart of a PhC biosensor. Note that the illustration was not drawn in scale with exact particle layers. (b) Formation of sandwich immunocomplexes on a PhC biosensor. (c) Schematic of an assembly of a complete LF microchip-enabled biosensor for tear-based DR screening.

To accomplish this, a 50-ml centrifuge tube was filled with a 1% (w/v) Teflon solution (AF1601S-6, Dupont, Wilmington, DE, USA). Next, two glass slides were individually immersed in the 1% Teflon solution for a few seconds, allowing for the deposition of a thin hydrophobic film on their surfaces. The hydrophobic coating on the glass slides prevented the PMMA nanoparticles from adhering to the surfaces. The 1% (w/v) Teflon was obtained by diluting the original 6% (w/v) Teflon liquid with the FC-70 solvent (3M, St. Paul, MN, USA) at a volumetric ratio of 1:5. Afterward, both the glass slides were slowly baked at 40 °C in an oven for 30 min to dry the surfaces. Subsequently, 200 μl of 2×10^{10} beads/ml PMMA nanoparticle suspension was concentrated in a 1.5 ml Eppendorf tube by centrifugation at 13 500 rpm for 8 min. After removing 120 μl of supernatant from the tube, 20 μl of the remaining suspension was sandwiched between the two hydrophobic glass slides separated with 1-mm spacers. The PMMA nanoparticles would self-assemble to form a face-center cubic (FCC) crystal lattice after water was completely evaporated by leaving the sandwich particle suspension at room temperature (25 °C) overnight. Then, the PMMA nanoparticle self-assembly was annealed in an oven at 115 °C for 10 min to consolidate the nanostructure (Fig. S4 in the supplementary material). During the heat treatment, the PMMA nanoparticles were expected to slightly melt and fuse with neighboring particles. The heat treatment conditions were determined after the treated PMMA self-assembly survived a shaker at 800 rpm for 8 h and 20 times of 5-s sonication. After cutting from the large assembly, a PhC substrate measuring 1 mm^2 was obtained. Finally, a 5-nm gold film was deposited on the top of the PhC substrate by an E-beam evaporator (EBC-12, ULVAC, Japan) to enable later antibody immobilization.

B. Preparations of an antibody-conjugated PhC substrate and probes

To enable the desired PhC biosensors, a PhC substrate conjugated with the capture antibody and fluorescent polystyrene (PS) particles conjugated with the probe antibody were prepared separately beforehand. Herein, a sandwich immunoassay was performed to capture the target biomarker protein, LCN-1 [Fig. 2(b)]. Thus, 4 μl of 0.1 μg/μl anti-LCN-1 polyclonal IgG (capture antibody) (ab87786, Abcam, Oxford) solution was prepared in a 1.5-ml Eppendorf tube and gently mixed with 14 μl of gold reaction buffer provided by a gold conjugation kit (ab154873, Abcam, Boston, MA). Then, the PhC substrate was incubated with the mixture in the Eppendorf tube on a shaker at 400 rpm and 25 °C for 3 h. Consequently, the captured antibodies were covalently bound on the gold surface of the PhC substrate. Afterward, 2 μl of gold quencher was added into the tube as a blocking agent to avoid nonspecific binding and then incubated on a shaker at 400 rpm and 25 °C for 1 h. Eventually, the PhC substrate was washed with PBST five times to remove unbound capture antibodies. Meanwhile, another anti-LCN-1 monoclonal IgG (probe antibody) (ab76611, Abcam, Oxford) was conjugated with 200-nm amine-modified yellow-green fluorescent polystyrene particles (FluoSphere™ F8764, 505/517, Thermo Fisher Scientific Inc., Waltham, MA). First, 5 μl of 1 mg/ml probe antibody was mixed with 25 μl of 10 mg/ml 1-ethyl-3-(3-dimethylaminopropyl)-carbodiimide (EDC) (A10807, Alfa Aesar, Haverhill, MA) and 25 μl of 10 mg/ml *N*-hydroxysulfosuccinimide (Sulfo-NHS) (24510, Thermo Fisher Scientific Inc., Waltham, MA) in a 1.5-ml Eppendorf tube. Then, the mixture was incubated on a shaker at 25 °C and 800 rpm for 15 min. Subsequently, 15 μl of phosphate-buffered saline (UR-PBS001, UniRegion Bio-Tech, Hsinchu, Taiwan) with Tween-20 (P5927, Sigma-Aldrich, St. Louis, MO) (PBST, 0.01% Tween-20 in 1× PBS), 100 μl of 50 mM 2-(*N*-morpholino) ethanesulfonic acid (MES) buffer (M3671, Sigma-Aldrich, St. Louis, MO), and 30 μl of the fluorescent PS particles (4.57×10^{10} particles/ml) were mixed in the same tube and incubated with the activated probe antibodies on a shaker at 4 °C and 800 rpm for 4 h. After incubation, the unbound probe antibodies were washed five times with PBST by centrifugation at 13 500 rpm for 8 min to complete the final probe antibody-conjugated PS particles.

C. Realization of PhC immuno-biosensors

With the previously prepared antibody-conjugated PhC substrate and probes, the PhC immuno-biosensors would exhibit intensified fluorescence as the probe antibody was captured on the PhC substrate in the presence of the target biomarker. The fluorescent intensity was proportional to the concentration of the target biomarker. To realize PhC immuno-biosensors, the LCN-1 was initially mixed with the probe antibody-conjugated PS particles to complete LCN-1 probe antibody immunocomplex particles to achieve the expected sandwich immunoassay. Subsequently, the immunocomplex particles were mixed with the capture antibody-coated PhC substrate and waited at room temperature (25 °C) for 15 min to allow full immunoreactions. After washing the substrate five times with PBST, the final sandwich immunocomplexes immobilized on the PhC substrate were eventually obtained. Therefore, immunofluorescence shown herein served as a test biosensor that was placed in the test region of the microchannel [Fig. 2(c)]. For a control biosensor, 10 μl of 0.1 mg/ml LCN-1 proteins were in advance conjugated with the capture antibody-coated PhC substrate in an Eppendorf tube and shaken at 800 rpm at room temperature (25 °C) for 4 h. Then, after washing away the residual unbound LCN-1 proteins from the substrate five times, the control biosensor was placed in the control region of the microchannel next to its test counterpart [Fig. 2(c)].

D. PhC biosensors integrated with an LF microchip

Eventually, a PMMA microchip [Fig. 2(c)] was designed and fabricated in this study to house the biosensors and facilitate operations. The capillary force was used as a major driving force to move a sample fluid from the inlet to the waste well at the end of the microchannel.[18] When the fluid front reached the waste well, an absorbent tissue would serve as a second-stage driving force to keep the fluid flowing until all the samples were drained out of the microchannel. Then, target proteins would be captured by biosensors as the fluid flew over the biosensors. The use of an absorbent tissue reduced the required length of the microchannel for capillary action and ensured that all sample fluids were able to come into contact with the PhC biosensors. Furthermore, 70 μl of previously prepared probe antibody-conjugated PS particles were lyophilized in the inlet well in a freeze dryer (FD4.5-8P-L, Dogger Science, New Taipei City, Taiwan) at −50 °C for 3 h. The microchip (Fig. S1

in the supplementary material) comprised a circular inlet well ($\phi = 10 \times 2\ mm^2$), a waste well ($20 \times 15 \times 1\ mm^3$), which was used to accommodate the absorbent tissue, and a microchannel connecting both wells ($15 \times 1 \times 0.3\ mm^3$). An additional microchannel measuring $5 \times 1.5 \times 0.8\ mm^3$ was used to position both PhC biosensors at the end of the straight microchannel. The top and bottom PMMA plates were engraved by a computer numerical control machine (EGX-400, Roland, Irvine, CA). After engraving, two PMMA plates were initially treated by an ultra-violet excimer (L12530-01, Hamamatsu, Shizuoka, Japan) for surface modification[19–21] for 1 min and then bonded together by heating them in an oven at 80 °C for 8 h. The optimal temperature and time were determined after trial and error because they gently softened the PMMA to promote the bonding. Eventually, test and control biosensors were placed into the sensing region by inserting them through the slit between the top and bottom layers, followed by an absorbent tissue to complete the device [Fig. 2(c)]. For fluorescent images recording, the entire microchip was placed under a fluorescent microscope (BX51, Olympus, Japan) equipped with a 10× objective, a filter cube (U-MWIB3, OLYMPUS, Tokyo, Japan), and a digital camera (FL3-U3-13S2C-CS, Point Grey) (Fig. S2 in the supplementary material). Finally, when a sample fluid was dropped into the inlet well, the images of test and control biosensors were recorded by the digital camera separately after 15 min. It is worth noting that as a disposable device, the cost of the overall PMMA microchip, including PhC biosensors, is less than 10 US dollar. The fluorescence readout equipment, consisting of a fluorescent microscope, a PC, and a digital camera, represents the major expense of the system. The cost of this equipment may vary depending on brands, functions, and optical quality. However, this investment is one-time and can be reused.

E. PhC effect and enhanced immunofluorescence

The self-assembled photonic crystal forms an FCC structure.[22] The reflective wavelength can be predicted by modified Bragg's law[23] as follows:

$$\lambda = \frac{2d_{hkl}}{m} \times \sqrt{n_{eff}^2 - \sin^2\theta}, \quad (1)$$

where d_{hkl} is the inter-planar spacing between planes with Miller indices h, k, and l, which can be expressed as $d_{hkl} = \frac{d_p\sqrt{2}}{\sqrt{h^2+k^2+l^2}}$; n_{eff} is the effective refractive index of the photonic crystals, which can be expressed as $n_{eff} = 0.74{n_{PMMA}}^2 + 0.26{n_{air}}^2$; m is the order of Bragg diffraction, θ is the incident angle for the normal incidence; d_p is the particle diameter; n_{PMMA} is the refractive index of PMMA; and n_{air} is the refractive index of air. Given that the PMMA nanoparticles were 215 nm in diameter and other conditions were $n_{PMMA} = 1.49$, $n_{air} = 1$, $h = 1$, $k = 1$, $l = 1$, $m = 1$, θ=0° in this study, the reflective wavelength was expected to be 484 nm. A spectrometer (QE Pro-FL, Ocean Optics, Orlando, FL) was used to measure the actual reflective light (Fig. S3 in the supplementary material). Under measurement, a halogen light source transmitted through the optical fiber probe of the spectrometer was illuminated perpendicular to the surface of a PhC biosensor. Then, the same probe received reflective light that resonates with Bragg's lattice from the PhC to be identified its peak wavelength.

Herein, the PhC nanostructure can resonate with fluorescence under enhanced excitation, which occurs when the incident light couples to the resonant mode of the nanostructure; in other words, the excitation wavelength (505 nm) of 200-nm yellow-green fluorescent PS particles is close to the diffractive wavelength (487 nm). The electric field on the surface of the photonic crystal will be enhanced, and the absorption efficiency of the fluorophores will increase. Consequently, the fluorophores can emit stronger fluorescent light.[24–26]

III. RESULTS AND DISCUSSION

A. Characterizations of the nanostructure of self-assembled particles

In this study, 215-nm PMMA nanoparticles were used to form a self-assembled PhC biosensor. Based on Eq. (1), the theoretical wavelength was estimated to be 484 nm under the conditions of $n_{PMMA} = 1.49$, $n_{air} = 1$, $h = 1$, $k = 1$, $l = 1$, $m = 1$, θ=0° while the actual reflective wavelength measured by a spectrometer shows a peak at 487 nm [Fig. 3(a)]. The slight discrepancy between the measured and the theoretical values was likely caused by the nonuniformity of the nominal particle size. After the heat treatment, the PhC self-assembly was consolidated; however, the peak of the refractive wavelength was also slightly shifted to 490 nm, thereby implying minor deformation in the nanostructure caused by the heat treatment. A thin layer of gold was coated on the top surface of the PhC substrate to facilitate later biological functionalization. The reflection spectrum [Fig. 3(b)] showed that the peak was shifted back to 487 nm and the light intensity declined with the increased gold film thickness likely caused by the surface plasmon resonance. Interestingly, no intensity difference was observed between reflections from the front and the back of the coated surface. The final gold film thickness was set to 5 nm to avoid serious light attenuation. Note that a thinner gold film can be attempted if microfabrication allows.

In addition, the crystalline nanostructures were verified with an atomic force microscope (AFM) (NTEGRA II, NT-MDT, Limerick, Ireland). The surface morphologies of PhCs in three conditions were examined, including before and after heat treatment as well as after gold deposition [Figs. 3(c)–3(e)]. No significant changes in the nanostructures were observed in all three conditions, which were consistent with the optical properties discussed in Figs. 3(a) and 3(b). Additionally, the cross-sectional morphology of the nanostructure was revealed by cutting the gold-coated PhC substrate [Fig. 3(f)]. The bright strip indicates where the gold film is while the layer on top of it is a black tape used to fixed the PhC substrate during cutting. The results confirmed that the PhC biosensors were well modified by the optimized heat treatment and gold deposition without seriously disrupting the anticipated PhC effect.

B. Evaluations of PhC biosensor

Thus, the PhC biosensor was initially processed in a tube in this stage to evaluate the sandwich immunoassay of the PhC

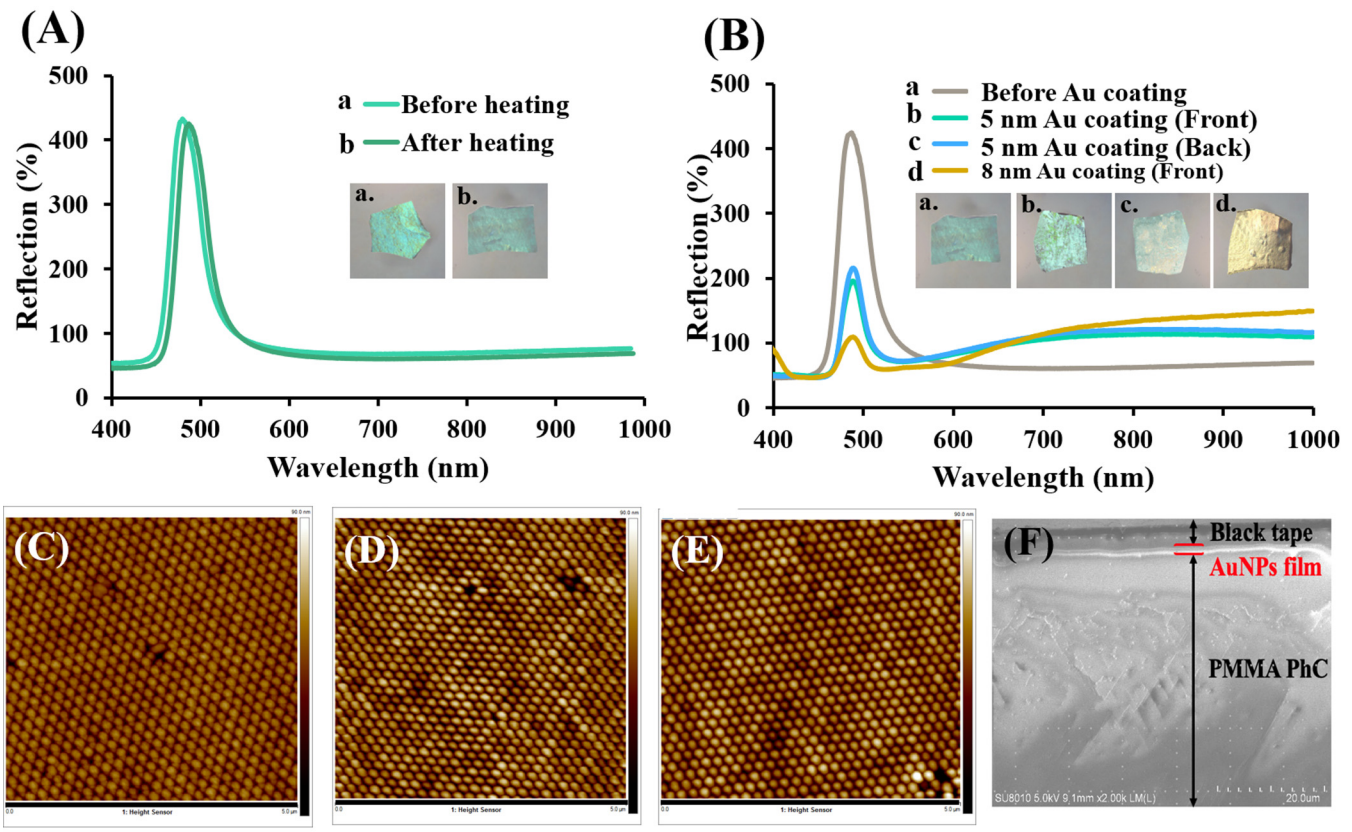

FIG. 3. Characterizations of the nanostructure of self-assembled particles. (a) Spectra of the self-assembled PMMA PhC before (peak at 487 nm) and after (peak at 490 nm) heating at 115 °C for 10 min. (b) Spectra of the self-assembled PMMA PhC before and after gold coating with thicknesses of 5 and 8 nm. No difference in intensity was found in the spectra of the front and back of the same PhC coated with a 5-nm gold film. AFM images of PhC nanostructures (c) before heating, (d) after heating without gold coating, and (E) after heating with 5-nm gold coating. The scale bars in all above AFM images are 5 μm. (f) SEM image of the cross-sectional PhC nanostructure. The black tape was used to fix the substrate during cutting.

biosensor and its immunofluorescence enhancement effect. A total of 20 μl of LCN-1 ranging from 1 to 100 μg/ml were investigated. Then, each of them was incubated on a shaker at 4 °C and 800 rpm for 4 h and then washed five times with PBST by centrifugation. Surface images of the PhC biosensors were taken by a fluorescence microscope to analyze their relative fluorescent intensities in the region of interest (ROI) where the area of each biosensor was included. The relative intensity was an ROI fluorescent intensity divided by the background value. Meanwhile, the control group was the PhC biosensor in the PBST solution without LCN-1. Both PhC and non-PhC groups were compared under the same condition [Fig. 4(a)]. Unlike the PhC biosensor, the non-PhC biosensor consisted of a simple gold film coated on a non-structural PMMA substrate, with antibodies conjugated to the gold surface. Notably, the PhC group exhibited higher fluorescence intensities than the non-PhC counterpart in all concentrations. The non-PhC group generally required at least tenfold higher concentration than the PhC group to achieve the same fluorescent intensity. In addition, both groups were proportional to the increased concentrations of LCN-1. Then, a calibration curve delineating the relationship between LCN-1 concentration and optical density (OD value) was conducted beforehand for validation using the bicinchoninic acid protein assay kit (J63283, Thermo Fisher Scientific Inc., Waltham, MA) [Fig. 4(b)]. Subsequently, a microplate reader (Infinite 200 Pro, Tecan, Männedorf, Switzerland) was used to validate supernatants from the above four concentrations of LCN-1 and the control after immunoassay in Fig. 4(a) based on calibration. The results confirmed the serially increased concentrations prepared for the LCN-1antigens and no different antigens were found between both PhC and non-PhC groups [Fig. 4(c)]. The equal intensities in both PhC and non-PhC groups reconfirmed the immunofluorescence enhancement shown in Fig. 4(a) resulted from the PhC effect.

For specificity, immunoassays of bovine serum albumin (BSA) and tumor necrosis factor-α (TNF-α) on the PhC biosensor were compared with that of the target protein LCN-1 at a fixed concentration of 0.1 mg/ml. Herein, the PBST served as a baseline, and all proteins were processed under the same condition as previous calibration. The result showed that the mean relative fluorescent

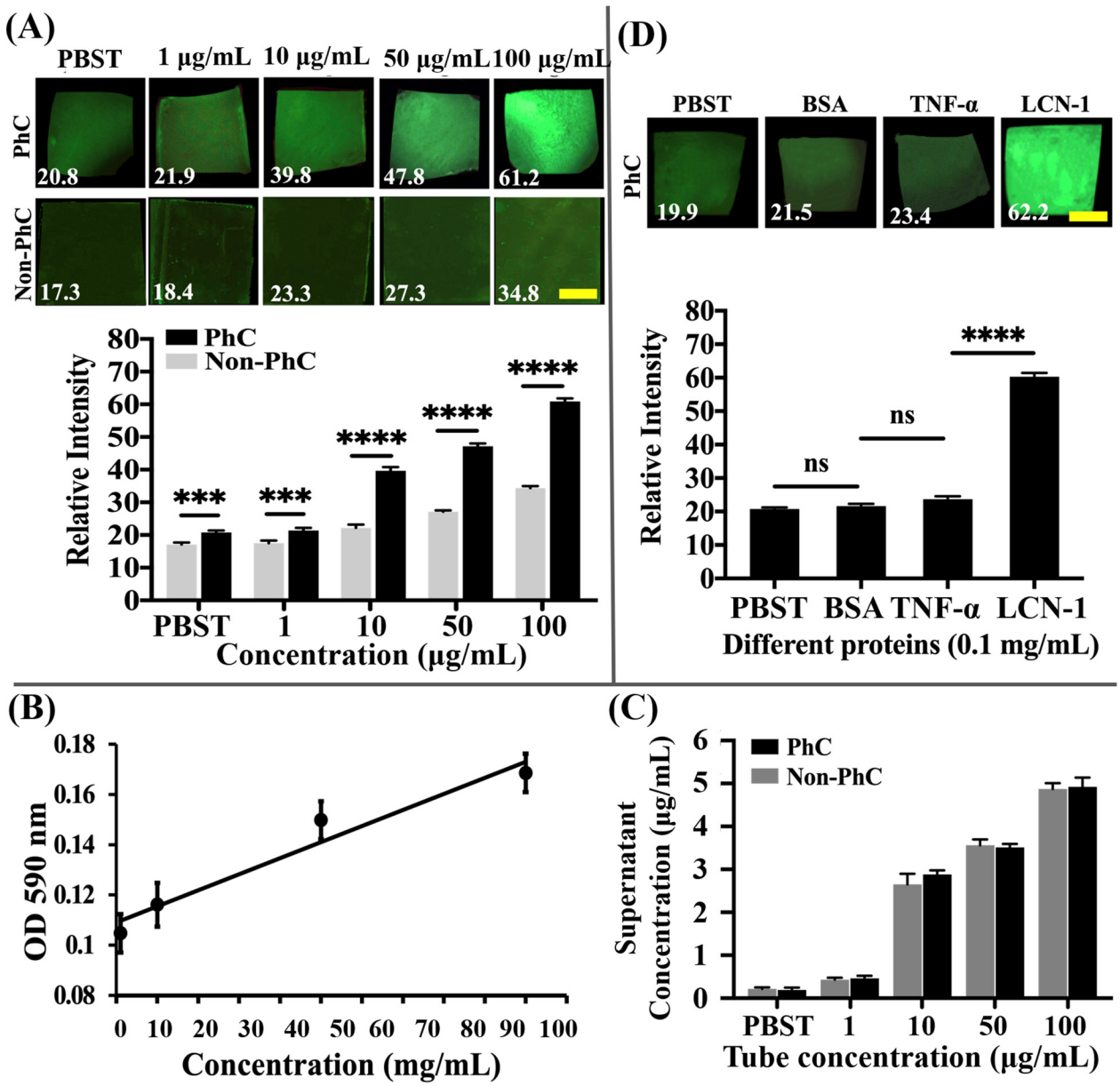

FIG. 4. Evaluations of the PhC biosensor in tubes. (a) Dose-dependent immunoassays and PhC-enhanced immunofluorescence with different LCN-1 concentrations. (n = 5) The insets above the bar chart are their corresponding fluorescent images of PhC. The numbers indicate their relative intensities. The scale bar is 500 μm. (b) Calibration line obtained from a microplate reader using a BCA protein assay kit. (c) Validation of the supernatants from the dose-dependent immunoassays by a microplate reader. (n = 3) The concentration was converted based on the calibration line. (d) Specificity tests with BSA, TNF-α, LCN-1, and without proteins (PBST only). (n = 3) The insets above the bar chart are their corresponding fluorescent images of PhC. The numbers indicate their relative intensities. The scale bar is 500 μm. Symbols "***," "****," and "ns" denote $p < 0.001$, $p < 0.0001$, and no significance, respectively, under the student's *t*-test. Error bars represent standard deviations.

intensity of the LCN-1 group was higher than others by nearly threefold at most, thereby indicating the high specificity [Fig. 4(d)]. However, the rest of the non-LCN-1 proteins exhibited low signal intensities as the baseline.

C. Effects of the LF microchip-enabled PhC biosensor

The optimized PhC biosensor was eventually embedded in an LF microchip to enable facile operations. Thus far, several volumes (20, 50, and 70 μl) of 0.05 mg/ml fluorescently labeled probe

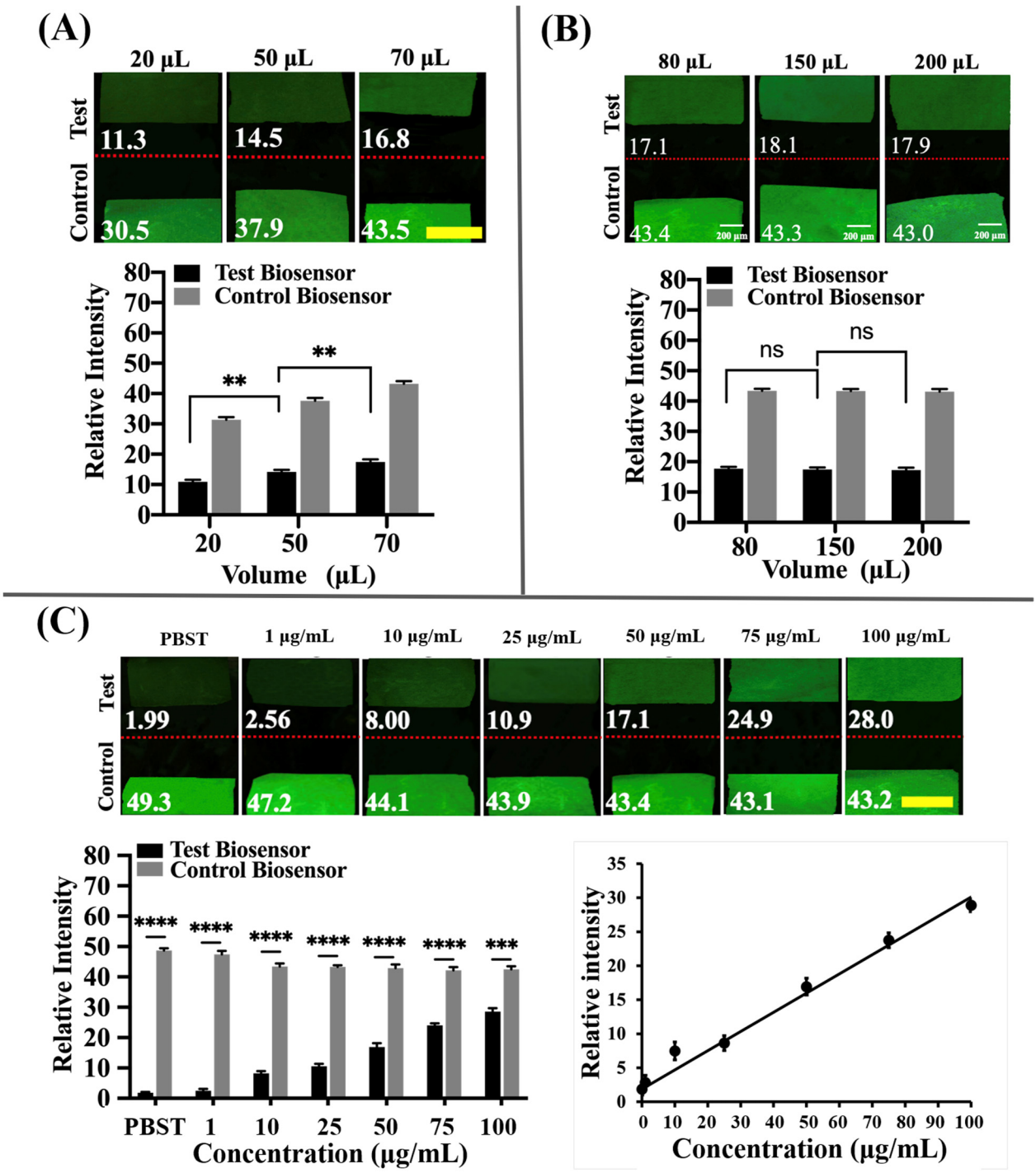

FIG. 5. Performances of the LF microchip-enabled PhC biosensor. (a) Determination of the optimal volume of the lyophilized material in the inlet of the microchip. (n = 3) (b) Determination of the optimal volume of samples required for testing. (n = 3) (c) Dose-dependent effect of the overall integrated PhC biosensor. The relative intensity escalates linearly with increased LCN-1 concentration between 1 and 100 μg/ml. (n = 3) Insets above the bar charts are their corresponding fluorescent images of PhC. The numbers indicate their relative intensities. Scale bars in all images are 500 μm. Symbols "**," "****," "*****," and "ns" denote $p < 0.01$, $p < 0.001$, $p < 0.0001$, and non-significant, respectively, under the student's *t*-test. Error bars represent standard deviations.

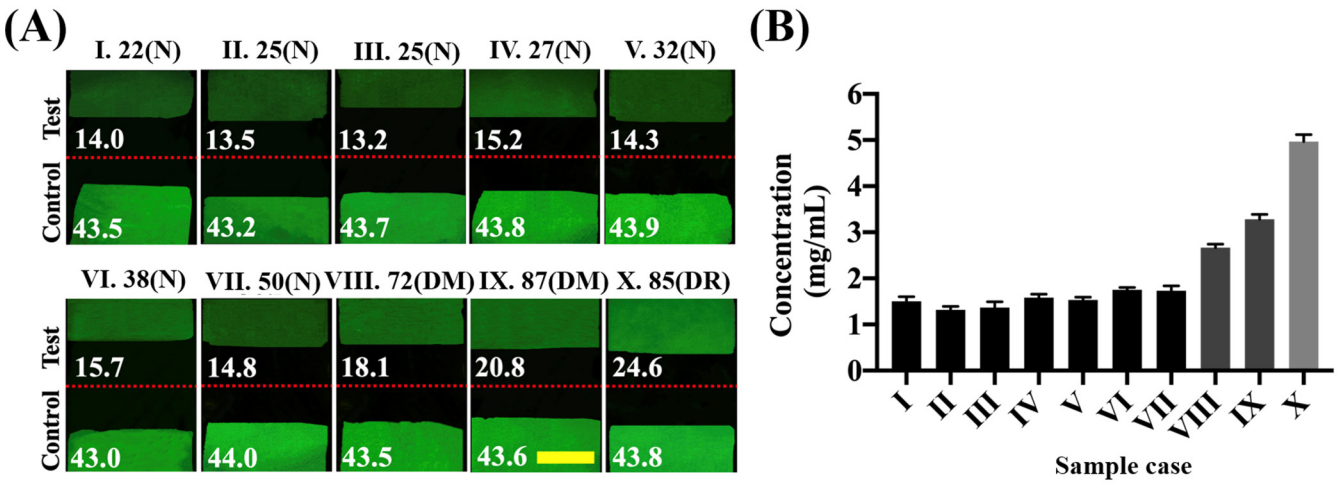

FIG. 6. Preclinical evaluation with ten human tear samples. (a) Fluorescent images of the test and control regions for 10 preclinical tests. The numbers shown in images denote their mean gray levels. The number on top of each image is the age of the subject. The letters in the parentheses denote their major medical conditions. N, No DR and DM; DM, diabetes mellitus; DR, diabetic retinopathy. The scale bar is 500 μm. (b) Concentrations of LCN-1in all cases measured from the LF microchip-enabled PhC biosensor. (n = 3) Error bars represent standard deviations.

antibodies were lyophilized in the inlet well of the microchip in advance. Lyophilization is a common technology used to prevent degradation, extend shelf life, and enhance stability of the biomaterial before reconstitution. The result indicated that a larger volume of lyophilized material, that is, fluorescently labeled probe antibody, was beneficial to a higher signal intensity [Fig. 5(a)]. Therefore, considering the maximum volume of the inlet well (78 μl), the optimal volume of the lyophilized material herein was determined to be 70 μl. As soon as a sample fluid was dropped into the microchip, the fluorescently labeled antibodies would be rapidly resuspended and mixed with the target protein LCN-1. In addition, the optimal sample fluid volume was evaluated. Three different volumes (80, 150, and 200 μl,) of 0.05 mg/ml LCN-1 solution were attempted. No significant differences were observed between the three volumes [Fig. 5(b)], thereby indicating saturation of lyophilized antibodies. Therefore, considering the possible scarcity of samples in some diseases, the sample volume was determined to be 80 μl in the following evaluations. In the real clinical practice for DR, the baseline of healthy people is around 1–2 mg/ml.[15,16] Consequently, only 10 μl tear fluid was needed per test. The final sample volume was readjusted to 80 μl by diluting with 70 μl of PBST.

Herein, six concentrations of LCN-1 in PBST ranging over 0.001, 0.01, 0.025, 0.05, 0.075, and 0.1 mg/ml plus their controls were investigated to evaluate the overall LF microchip-enabled PhC biosensor [Fig. 5(c)]. The final readout was determined in 15 min. The controls at all LCN-1 concentrations showed positive signals, thereby validating their successful testing on the microchip. The relative intensity linearly escalated with the increased LCN-1 concentration between the tested range. The intensity of the control was prone to slightly decrease with the increased LCN-1 concentration because of the competitive immunoassay for probe antibodies between the test and control PhC biosensors. The test PhC initially captured the antibodies because it was positioned before the control PhC biosensor. The linearity of the immunofluorescence and the LCN-1 concentration proved the feasibility of the LF microchip-enabled PhC biosensor for potential DR screening. Moreover, the LoD of the device reached 3 μg/ml under the three standard criteria.

D. Preclinical evaluation with human tear samples

For the proof of concept, ten human tear samples were collected from volunteers and tested with the LF microchip-enabled PhC biosensor. Tear samples were obtained through a glass capillary (Fig. S5 in the supplementary material) at the Department of Ophthalmology, National Cheng Kung University Hospital (NCKUH) under an IRB Agreement No. B-ER-112-052. Exclusion criteria included dry eye syndrome, macular degeneration, under drug treatments, and sleep less than 8 h. First, the lower eye lid was pulled downward, revealing the conjunctival sac into which the glass capillary was held horizontally. Due to the capillary effect, the tear fluid then flowed into the glass capillary. Finally, the tear sample was pipetted out of the glass capillary into a microcentrifuge tube and stored in a refrigerator for later use. The sample collection was conducted by a specialist in the laboratory. The ages of the volunteers ranged from 22 to 87 years old. The ratio of males to females was 1:1. Six of the ten samples were from healthy volunteers (cases I–VI). Notably, cases III and VI had a family history of diabetes but no personal history of diabetes mellitus (DM). Case VII was diagnosed with hypertension and had a family history of DM but no personal history of DM or DR. Cases VIII and IX had confirmed diagnoses of diabetes. Case X had confirmed diagnosis of DR. The medical information was primarily obtained through their questionnaires (Tables S1 and S2 in the supplementary material).

10 μl of the collected tear fluid was first diluted 50-fold with PBST in a microcentrifugal tube before measurement. Next, 80 μl of the diluted sample was dropped into the inlet well of the microchip for testing. After 15 min, the microchannel was washed by flowing 80 μl of PBST five times to remove unbound proteins. The fluorescence intensities of the test and control regions were captured by a fluorescence microscope [Fig. 6(a)]. The bright fluorescence of the control region confirmed the validity of all the tests. In the healthy subjects (I–VI), the measured concentrations of LCN-1 were between 1.3 and 1.7 mg/ml [Fig. 6(b)], which remained in the range of healthy baselines around 1–2 mg/ml.[15,16] Although cases III and VI had a potential risk factor of getting DR owing to their family history of diabetes, there seemed no signs of DR at the moment of testing, probably due to their young ages. It was also found that case VII, who had hypertension, seemed to show a low risk of DR according to their concentration of LCN-1 [Fig. 6(b)]. The low concentration implied that LCN-1 was not altered by the DR-irrelevant disease. By contrast, the concentrations of LCN-1 in the diabetic cases VIII and IX escalated to 2.7 and 3.4 mg/ml, respectively [Fig. 6(b)]. The significant increases in LCN-1 against the healthy subjects indicated their high risks of getting DR; hence, appropriate medical interventions were highly suggested. In the final DR-confirmed case X, the concentration of LCN-1 reached 4.8 mg/ml, which was the highest concentration among all the tested cases [Fig. 6(b)]. The result was consistent with their revealed medical history of 30 years of chronic diabetes and 5 years of DR. Through the preclinical evaluation, the clinical feasibility of the LF microchip-enabled PhC biosensor was proven.

IV. CONCLUSIONS

DR is non-lethal; however, it is a costly diabetic complication worldwide. The rapidly increasing diabetic population has exacerbated the situation even more. Therefore, early eye screening can effectively procrastinate or prevent the disease from rapid deterioration and greatly improve the patient's life quality. Unfortunately, the current ophthalmologic examinations, such as ophthalmoscopy, FAG, or OCT, are either time-consuming, labor-intensive, invasive, or too costly. Thus, a 3D PhC biosensor integrated with an LF microchip was developed in this study to address the abovementioned challenges. The PhC biosensor was made up of 215-nm PMMA nanoparticles by self-assembly, thereby forming an FCC nanostructure, and then annealed to consolidate its mechanical stability. The compact device was disposable and allowed non-invasive samples from tears to facilitate the DR screening. The LF microchip enabled the fluid to be self-driven into the microchannel and achieved immunoassays on the PhC biosensor in 15 min. A more than tenfold enhancement in concentration was achieved with PhC compared to non-PhC in order to reach the same equivalent signal intensity. In addition, the specificity evaluation corroborated that the PhC biosensor was specific to the target protein LCN-1. In addition, a calibration of the overall LF microchip-enabled PhC biosensor was conducted with concentrations of LCN-1 ranging from 1 to 100 μg/ml. Moreover, an optimal LoD of 3 μg/ml was obtained based on the three standard deviation criteria. Finally, a preclinical evaluation was conducted using ten tear samples from volunteers. The results showed that the concentrations of LCN-1 in cases with chronic diabetes or DR were at least twofold higher than in healthy or non-diabetic cases. This trend was consistent with their medical conditions. Overall, this preliminary study provided insight into the future rapid tear-based DR screening with the proposed device.

SUPPLEMENTARY MATERIAL

See the supplementary material for dimensions of LF microchip (Fig. S1), experimental setup (Figs. S2 and S3), heat treatments of annealed PhC (Fig. S4), tear fluid collection (Fig. S5), and questionnaires from volunteers (Table S1).

ACKNOWLEDGMENTS

This research was supported by the Ministry of Science and Technology, Taiwan under Grant No. 112-2221-E-006-018-MY3 and the Chi-Mei Medical Center under the Collaborative Grant No. CMNCKU11112.

AUTHOR DECLARATIONS

Conflict of Interest

The authors have no conflicts to disclose.

Ethics Approval

The tear samples were obtained from the Department of Ophthalmology, National Cheng Kung University Hospital (NCKUH) under an IRB Agreement No. B-ER-112-052. Exclusion criteria included dry eye syndrome, macular degeneration, under drug treatments, and sleep less than 8 h.

Author Contributions

Li-Ying Chen: Conceptualization (supporting); Data curation (lead); Formal analysis (equal); Investigation (equal); Validation (equal); Visualization (lead); Writing – original draft (supporting). **Sheng-Min Hsu:** Conceptualization (supporting); Data curation (supporting); Investigation (supporting); Resources (supporting); Writing – review & editing (supporting). **Jhih-Cheng Wang:** Conceptualization (equal); Funding acquisition (equal); Project administration (equal); Resources (equal); Validation (equal); Writing – review & editing (equal). **Tai-Hua Yang:** Funding acquisition (supporting); Resources (supporting); Validation (supporting); Writing – review & editing (supporting). **Han-Sheng Chuang:** Conceptualization (equal); Funding acquisition (equal); Investigation (equal); Methodology (equal); Project administration (equal); Resources (equal); Supervision (equal); Validation (equal); Visualization (equal); Writing – original draft (equal); Writing – review & editing (equal).

DATA AVAILABILITY

The data that support the findings of this study are available within the article and its supplementary material.

REFERENCES

[1] P. H. Scanlon, Curr. Diabetes Rep. **17**, 96 (2017).

[2]J. B. Skaggs, X. Zhang, D. J. Olson, S. Garg, and R. M. Davis, N. C. Med. J. **78**, 121–123 (2017).
[3]R. K. Lord, V. A. Shah, A. N. San Filippo, and R. Krishna, Ophthalmology **117**, 1274–1274.e3 (2010).
[4]T. Nazir, M. Nawaz, J. Rashid, R. Mahum, M. Masood, A. Mehmood, F. Ali, J. Kim, H.-Y. Kwon, and A. Hussain, Sensors **21**, 5283 (2021).
[5]C. H. Tan, W. H. Quah, C. S. H. Tan, H. Smith, and L. Tudor Car, BMJ Open **9**(12), e028811 (2019).
[6]U. Iqbal, Int. J. Retina Vitr. **7**, 44 (2021).
[7]J. R. Sempionatto, L. C. Brazaca, L. García-Carmona, G. Bolat, A. S. Campbell, A. Martin, G. Tang, R. Shah, R. K. Mishra, J. Kim, V. Zucolotto, A. Escarpa, and J. Wang, Biosens. Bioelectron. **137**, 161–170 (2019).
[8]J. Xu, X. Tao, X. Liu, and L. Yang, Anal. Chem. **94**, 8659–8667 (2022).
[9]M. Senior, Nat. Biotechnol. **32**, 856 (2014).
[10]R. C. Tseng, C.-C. Chen, S.-M. Hsu, and H.-S. Chuang, Sensors **18**, 2651 (2018).
[11]D. H. Keum, S.-K. Kim, J. Koo, G.-H. Lee, C. Jeon, J. W. Mok, B. H. Mun, K. J. Lee, E. Kamrani, C.-K. Joo, S. Shin, J.-Y. Sim, D. Myung, S. H. Yun, Z. Bao, and S. K. Hahn, Sci. Adv. **6**, eaba3252 (2020).
[12]J.-Y. Wang, J.-S. Kwon, S.-M. Hsu, and H.-S. Chuang, Lab Chip **20**, 356–362 (2020).
[13]W.-L. Chen, M. Jayan, J.-S. Kwon, and H.-S. Chuang, Biosens. Bioelectron. **193**, 113527 (2021).
[14]K.-C. Wang, A. Kumar, S. J. Williams, N. G. Green, K. C. Kim, and H.-S. Chuang, Lab Chip **14**, 3958–3967 (2014).
[15]J. M. Tiffany, Dev. Ophthalmol. **41**, 1–20 (2008).
[16]É. Csősz, P. Boross, A. Csutak, A. Berta, F. Tóth, S. Póliska, Z. Török, and J. Tőzsér, J. Proteomics **75**, 2196–2204 (2012).
[17]J.-C. Wang, H.-Y. Ku, T.-S. Chen, and H.-S. Chuang, Biosens. Bioelectron. **89**, 701–709 (2017).
[18]W. Hua, W. Zhou, W. Wang, Z. Wang, R. Wu, and L. Zhu, SN Appl. Sci. **3**, 315 (2021).
[19]C. W. Tsao, L. Hromada, J. Liu, P. Kumar, and D. L. DeVoe, Lab Chip **7**, 499–505 (2007).
[20]V. Sood, *An Experimental Study on Thermal Bonding Effects of PMMA Based Micro-Devices Using hot Embossing* (The University of Texas at Arlington, 2007).
[21]C. Wochnowski, M. A. Sham Eldin, and S. Metev, Polym. Degrad. Stab. **89**(2), 252–264 (2005).
[22]E. W. Seelig, B. Tang, A. Yamilov, H. Cao, and R. P. H. Chang, Mater. Chem. Phys. **80**, 257–263 (2003).
[23]T. Tchen, Tech. Phys. Lett. **29**, 235–236 (2003).
[24]N. Ganesh, W. Zhang, P. C. Mathias, E. Chow, J. A. N. T. Soares, V. Malyarchuk, A. D. Smith, and B. T. Cunningham, Nat. Nanotechnol. **2**, 515–520 (2007).
[25]Y. Xiong, Q. Huang, T. D. Canady, P. Barya, S. Liu, O. H. Arogundade, C. M. Race, C. Che, X. Wang, L. Zhou, X. Wang, M. Kohli, A. M. Smith, and B. T. Cunningham, Nat. Commun. **13**, 4647 (2022).
[26]N. Ganesh, P. C. Mathias, W. Zhang, and B. T. Cunningham, J. Appl. Phys. **103**, 083104 (2008).